

SOLUTIONS FOR THE METAL-BATH INTERFACE IN ALUMINIUM ELECTROLYSIS CELLS

Valdis Bojarevics and Koulis Pericleous

University of Greenwich, School of Computing and Mathematical Sciences,
30 Park Row, London, SE10 9LS, UK
V.Bojarevics@gre.ac.uk

Abstract

The dynamic MHD modelling package is applied to the simple test case presented recently by Severo, et al. in Light Metals 2008 [1]. The electrolyte channel effect is demonstrated to have a crucial effect determining the shape and size of the metal-bath interface deformation. A simple shallow water model allowing account of the channels is proposed. The problem is extended by a model of busbars in order to run the universal busbar design tool and to apply it for the dynamic simulations. The interface stability is tested and compared for the channel effects. Results indicate a rotating wave instability without the channels and a sloshing wave instability with the channels.

Introduction

The MHD problem for aluminium electrolysis cells is of increasing importance due to significant electrical energy costs, disruptions in the technology and control of environmental pollution rate. The electric current with the associated magnetic field create effects limiting the cell productivity and possibly cause an instability of the interface between liquid aluminium and electrolyte. Moreau and Evans [2] applied the linear friction model for the horizontal circulation velocity and introduced models for the electrolyte channels surrounding the anodes, their influence on the circulation and the metal-bath interface deformation. Actually, the linear friction and the variable bottom effects are used widely in the sea wave theoretical studies [3]. The linear friction is a simplification of the more general nonlinear bottom friction term appearing in the shallow water models [4].

According to the Moreau and Evans [2] the interface deformation in the stationary case increases very significantly when the electrolyte channels are accounted. However for unstationary or stability problems in the aluminium electrolysis cells the models used are typically restricted to the mathematical developments without the inclusion of the electrolyte channels, see for example [5-8]. Recently a theory and numerical model of the 'shallow layer' electrolysis cell was extended to the cases of variable bottom of aluminium pad and the variable thickness of the electrolyte due to the anode nonuniform burn-out process and the presence of the side channels[9]. However, in the theoretical development [9] the free surface presence in the electrolyte channels was not accounted for, effectively assuming that the rigid lid surface condition is imposed for the channels and the anode bottom.

The problem of the interface calculation appeared in the light of the recent paper [1] providing a clear 'benchmark' test for the stationary interface and the velocity field in the liquid metal. During the first attempts to apply the numerical model [9] we

obtained an interface shape which was quite different from that presented in [1], therefore we reconsidered the theory by including the free surface effects for the bath filled deep channels. The inclusion of the channels permits to develop a simple extension of the shallow water theory. The new version is directly applicable to the previous full nonlinear wave model and the dynamic interaction with the electromagnetic field as it is implemented in the MHD numerical code.

Mathematical model for the deformation of interface between two liquid shallow layers

The full description of the theory is given in the previous publications, see [9] and the references therein. Here we will repeat just the main points in the derivation and will stress the differences introduced by the free surface on the top of the channels. In the present extension of the theory for a variable layer depth we will assume that the layer deformation is small, except for the channels whose effect will be expressed as a hydrostatic 'connected vessels' principle. The shallow water model derivation starts with the assumption that the vertical momentum equation for a small depth fluid reduces to quasi-hydrostatic equilibrium between the vertical pressure p and the gravity g :

$$0 = -\partial_z p - \rho g \quad (1)$$

Then formally integrating, the pressure at any level z is

$$p(x, y, z) - p(H) = -\rho g(z - H), \quad (2)$$

where the reference height $H(x,y,t)$ can be chosen as the common surface for both liquid layers – the unknown interface between the metal and bath. The hydrostatic pressure distribution gradient in the horizontal direction does not depend on vertical coordinate in the respective layer, as can be seen from (2):

$$\begin{aligned} \partial_x p(x, y, z) &= \partial_x p(H) + \rho g \partial_x H \\ \partial_y p(x, y, z) &= \partial_y p(H) + \rho g \partial_y H \end{aligned} \quad (3)$$

If the top surface of the bath layer is H_t , then the pressure at the top of rigid lid enclosed channels will be obtained from the full solution. However, if there is a free surface on top of the bath channels, then $p(H_t) = 0$, and the pressure at the variable interface H is related by the hydrostatics to the local position only:

$$p(H) = \rho_2 g(H_t - H(x, y, t)), \quad (4)$$

where for clarity we added the index '2' for the bath layer properties. According to the Moreau & Evans [2], the surface H_i in the channels is practically flat and equal in all channels. If the channels (side, middle and between the individual anodes) are sufficiently deep, say 2-3 or more times the ACD, then this hydrostatic pressure will effectively act in all electrolyte layer, similarly to connected vessels principle. The electromagnetic force in the electrolyte will give very little modification to this dominant hydrostatic pressure. Then from (4) follows an approximated pressure gradient variation in the electrolyte at the variable interface $H(x,y)$:

$$\begin{aligned}\partial_x p(H) &= -\rho_2 g \partial_x H \\ \partial_y p(H) &= -\rho_2 g \partial_y H\end{aligned}\quad (5)$$

The equations (5) are approximate to the order of the H_i deviation from the constant value at the free surface contacting the surrounding air.

Having stated the approximations for the pressure and its horizontal gradient (3) in both the shallow layers, we can state the horizontal momentum equations for the depth average non-dimensional quantities. For simplicity we will consider initially the stationary case only. The Moreau & Evans model [2] is based on the linear equations for the two fluid layers:

$$0 = -\partial_j p - \mu \hat{u}_j + \hat{f}_j, \quad (6)$$

$$\partial_j \hat{u}_j = 0, \quad (7)$$

where the indexes $j = (1 \text{ or } 2)$ represent respectively x, y coordinates, the summation over repeated indexes j means the divergence free depth average velocity field. After substituting the depth independent pressure gradient from (3), the horizontal momentum equations are

$$0 = -\partial_j p(H) - \rho_i g \partial_j H - \mu \hat{u}_j + \hat{f}_j. \quad (8)$$

The common pressure $p(H)$ at the interface can be eliminated by taking the difference between the equations in the two layers, characterized each by the respective index: $i=1$ (aluminium) and $i=2$ (electrolyte). The unknown interface shape will be determined by solving the resulting equations coupled to the velocity field. When the channels are absent, the friction coefficient can be assumed as a constant in each layer, and the equation (7) gives the second order equation for the interface:

$$(\rho_1 - \rho_2) g \partial_{jj} H = \partial_j (\hat{f}_{j1} - \hat{f}_{j2}). \quad (9)$$

The boundary conditions are derived from the zero normal velocity condition at the cell walls.

However, in the presence of the bath channels the approximation of a constant friction is not valid, dropping to a very low value in the channels. Therefore the divergence operator applied to (8) will not eliminate the velocity field from the interface equation. The coupling to the intense velocity near the channels can be eliminated, to a certain approximation discussed previously, if

applying the hydrostatic pressure gradient (5) directly in the equation (8) stated for the aluminium ($i = 1$) layer only:

$$0 = -(\rho_1 - \rho_2) g \partial_j H - \mu_1 \hat{u}_{1j} + \hat{f}_{1j}. \quad (10)$$

The continuity of the pressure at the interface is satisfied by choosing the pressure $p(H)$ at the common interface. The bottom friction in the aluminium is constant according to the Moreau & Evans model, and the divergence of (10) gives the stationary interface equation for the conditions with free surface deep electrolyte channels :

$$(\rho_1 - \rho_2) g \partial_{jj} H = \partial_j (\hat{f}_{j1}). \quad (11)$$

The horizontal circulation velocities, driven by the rotational part of the electromagnetic force, can be calculated by solving the equations (6) in the two layers. The numerically efficient procedure consists of taking first the curl of the equation (6) with a generalized coordinate dependent friction coefficient. Additionally, the 2-equation turbulence model can be applied for the horizontal turbulent momentum diffusion (the effective viscosity) in more general approach. We will not consider here this part of the theory, instead focusing on the interface evolution equation modification.

Taking into account the hydrostatic pressure distribution in the presence of the channels for the full time dependent interface equation stated previously [9], we have the non-linear wave equation for the aluminium-electrolyte interface $H(x,y,t)$ with the variable bottom $H_b(x,y)$ and top $H_t(x,y)$:

$$\begin{aligned}& \left(\frac{\rho_1}{H-H_b} + \frac{\rho_2}{H_t-H} \right) \partial_{tt} H + \left(\frac{\rho_1 \mu_1}{H-H_b} + \frac{\rho_2 \mu_2}{H_t-H} \right) \partial_t H - \\ & - (\rho_1 - \rho_2) g \partial_{jj} H = \\ & = \partial_j (-\hat{f}_{j1}) - \frac{1}{2} (H-H_b) \partial_{jj} \hat{f}_{z1} - \\ & - [\rho_1 \partial_j (\hat{u}_{k1} \partial_k \hat{u}_{j1}) - \rho_2 \partial_j (\hat{u}_{k2} \partial_k \hat{u}_{j2})]\end{aligned}\quad (12)$$

The linear stability models can be recovered from (12) by excluding the nonlinear horizontal velocity term (containing the rotational and potential parts), the vertical electromagnetic force component \hat{f}_z contribution, and assuming the H_b and H_t as constants. The nonlinear equation (12) extends the wave description to the weakly nonlinear and slowly varying top and bottom cases in the presence of electrolyte channels. The complexity of any practically usable MHD model arises from the coupling of the various physical effects: fluid dynamics, electric current distribution, magnetic field and thermal field. Magnetic field in an aluminium cell is created by the currents in the cell itself and from the complex bus-bar arrangement around the cell, in the neighboring cells and the return line, and by the effect of cell construction steel magnetization. The general MHD model, presented previously [9,10], accounts for the time dependent coupling of the current and magnetic fields with the bath-metal interface movement. The magnetic field from the currents in the full bus-bar network is recalculated at each time step during the dynamic simulation using the Biot-Savart law.

Results for the 180 kA benchmark cell

The numerical solution of the described MHD model uses a mesh of 128x64x2 and a spectral function representation in the space of each fluid layer. This ensures a good accuracy solution and enables one to re-compute the electromagnetic and fluid dynamic field time dependent distribution in a reasonable computational time if required. The paper [1] provides several ‘benchmark’ tests for the aluminium electrolysis cell MHD models regarding the stationary fields only. The first test is for a given electromagnetic force distribution in the aluminium layer only. In this case both equations (9) and (11) are equal and the results computed with our MHD code are presented in the Figure 1, showing practically identical correspondence to the analytical result given in [1].

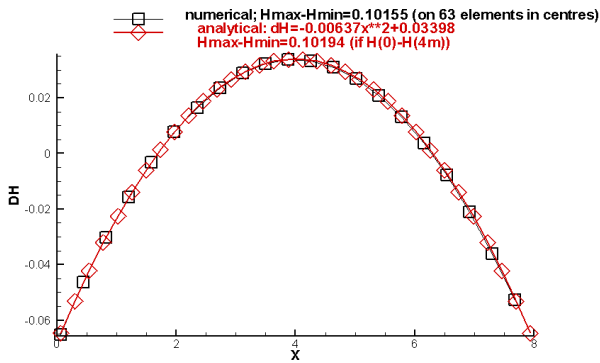


Figure 1. The test N 1 for the interface shape of a given electromagnetic force in the aluminium layer only.

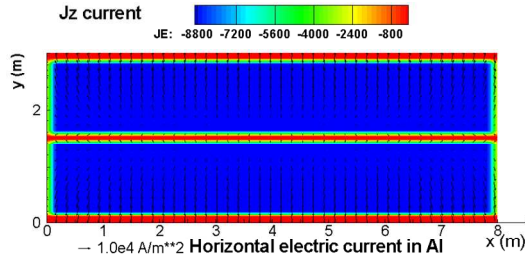


Figure 2. The computed electric current in the electrolyte with the channels.

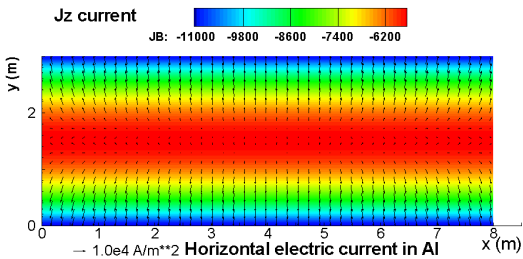


Figure 3. The computed electric current in the liquid metal with the prescribed bottom distribution.

The second test requires to compute the electric current in both fluid layers from the given distribution at the top (uniform from all anodes) and the bottom as

$$j_z = -5625 - 2500y^2 \text{ (A/m}^2\text{)}, \quad (13)$$

where the coordinate origin is the middle of the flat bottom of the cell. The electric current computed by the MHD code for these conditions is represented in the Figures 2 and 3. The presence of the channels is clearly seen for the electrolyte layer in the Figure 2. The magnetic field is assumed to be given in both fluid layers independent of the vertical coordinate z :

$$\begin{aligned} B_x &= 6y \cdot 10^{-3} \text{ (T)} \\ B_y &= (-3x + 1.5) \cdot 10^{-3} \text{ (T)} \\ B_z &= (xy + 0.5) \cdot 10^{-3} \text{ (T)} \end{aligned} \quad (14)$$

The $\text{div } \mathbf{B} = 0$ for this field, but the Ampere equation $\text{curl } \mathbf{B}/\mu_0 = \mathbf{j}$ gives the current in the fluid:

$$\mathbf{j} = \mathbf{e}_x 10^3 x - \mathbf{e}_y 10^3 y - \mathbf{e}_z 9 \cdot 10^3 \text{ (A/m}^2\text{)}, \quad (15)$$

which is not very realistic and does not correspond to the given conditions at the top and bottom. Nevertheless, the magnetic field (14) is thought to be representative for a typical 180 kA cell. The given by (14) magnetic field is represented in the Figure 4.

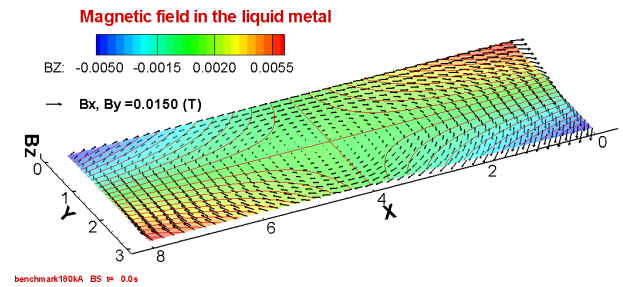


Figure 4. The magnetic field of the prescribed distribution.

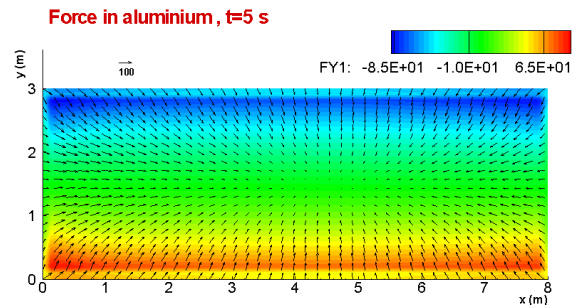
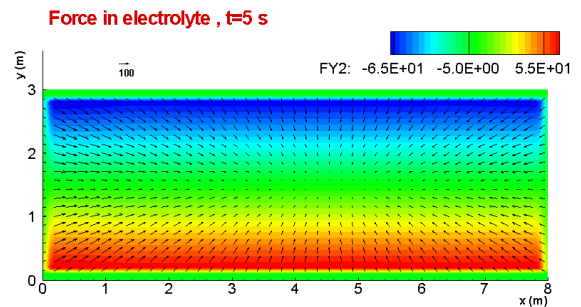


Figure 5. The electromagnetic force distribution including the electrolyte channels.

The electromagnetic force distribution computed for the given magnetic field and the electric current (shown in Figures 2 and 3) is demonstrated in the Figure 5. Clearly, there are no electromagnetic force in the electrolyte channels, but the overall force distribution and magnitude are quite similar in both layers. Therefore it is not surprising to find the interface deformation being very small and slightly inflected in the middle (because of the larger electrolyte force concentration there) as shown in the Figure 6 for the case without the effect of the electrolyte channel free surface. There is practically a balance between the ‘pinching’ effects of the forces in the two layers. A strikingly different interface deformation (Figure7) is obtained when using the model equation (11) with the hydrostatic pressure dominating in the electrolyte. For the comparison with the published ‘benchmark’ results [1] the Figure 8 shows a very close correspondence with the presented theory and numerical result.

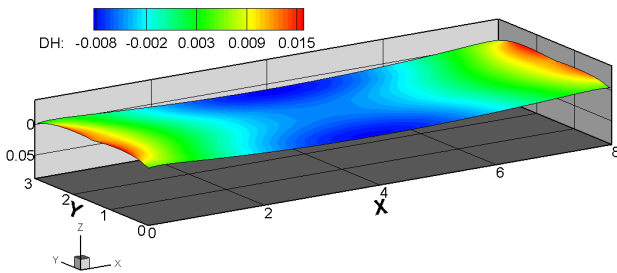


Figure 6. The computed metal-bath shape without the open channel effect.

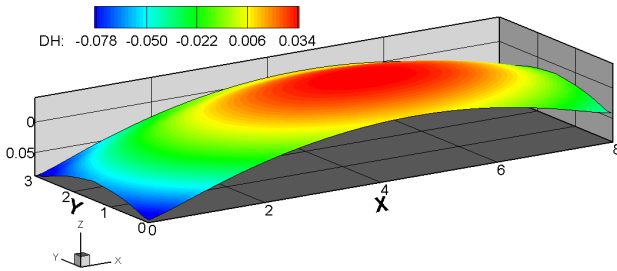


Figure 7. The computed metal-bath shape with the open channel effect.

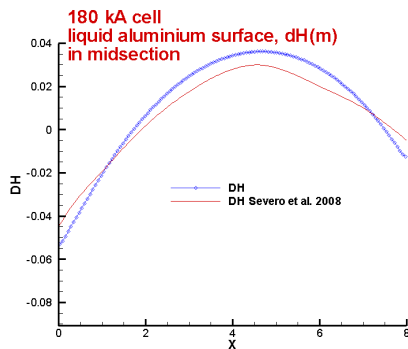


Figure 8. The computed metal-bath shape at the cell middle section in longitudinal direction compared to the result of [1].

The accurate representation of the interface depends on a number of additional conditions, like for instance, the anode bottom being burnt out to the profile corresponding to the actual interface and corresponding electric current redistribution for the constant ACD, see Figure 9 for the anode bottom computed with the MHD code.

For further tests the velocity fields were computed. The velocity in the electrolyte is not shown in [1], but the initial distribution computed with the presented here MHD code (Figure 10) is very similar qualitatively to that predicted by Moreau & Evans [2], clearly showing the effects of the intense recirculation in the channels. The flow is sufficiently intense and develops significant turbulence, which is represented by the turbulent kinetic energy distribution in the Figure 10. The momentum diffusion and advection (not accounted for in [2]) leads to a redistribution of the velocity field, as shown in the Figure 11. A very similar transformation of the velocity field is found for the aluminium layer, as shown in Figures 12 and 13. The established velocity field is very similar to that predicted in [1] as a part of the ‘benchmark’ tests.

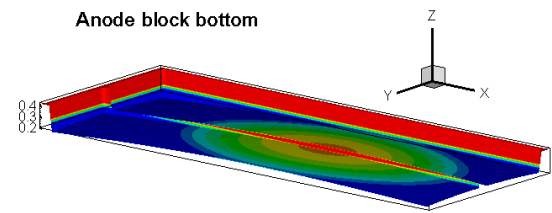


Figure 9. The burn-out effect on the anode block bottom.

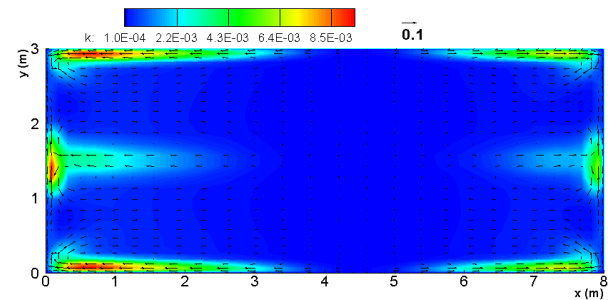


Figure 10. Initial velocity in the bath, 5s.

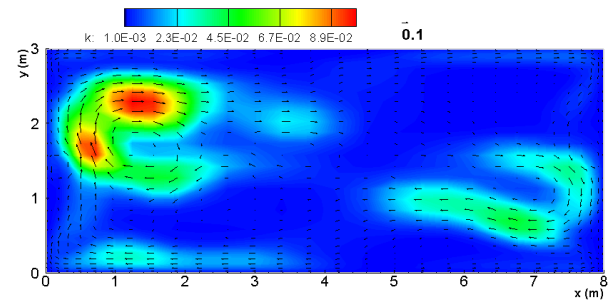


Figure 11. Established velocity in the bath, 100s.

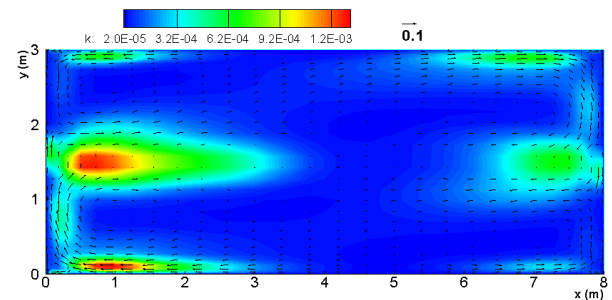


Figure 12. Initial velocity in the liquid metal, 5s.

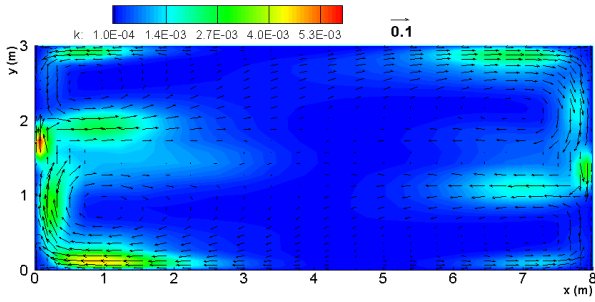


Figure 13. Established velocity in the liquid metal, 100s.

Since we have derived a new modification of the time dependent interface model, given by the equation (12), we need to investigate the consequences of the free surface channels on the possibly unstable behavior of the electrolysis cell. For this purpose a model bus network for a 180 kA cell was set up, as shown in the Figure 14. This permits to run the full MHD time dependent code with coupling of the fields. The magnetic field (without the effect of any steel parts) is shown in the Figure 15 for the top of the liquid metal. The horizontal electric currents in the liquid affect the magnetic field, making it different at the top and bottom of the metal layer, as can be seen from the comparison of the Figures 15 and 16.

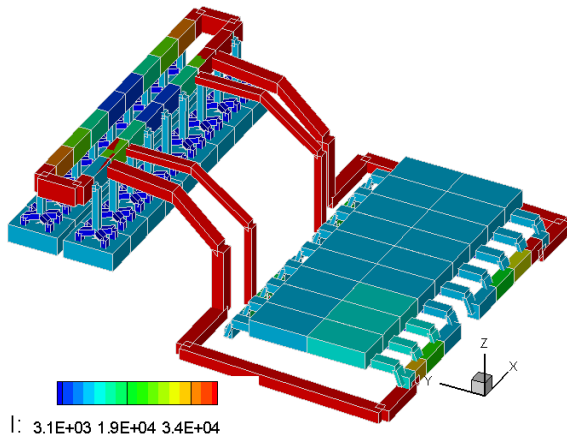


Figure 14. Busbar for the 180 kA cell used to simulate the 'benchmark' case.

For this model cell the initial deformation of the liquid metal surface (usually assumed to be a 'stationary' interface), as computed with the effect of the free electrolyte channels, is rather moderate if compared to the very large deformation computed for the 'benchmark' case. The reason for this is the significantly lower magnetic field B_z component in this more realistic cell model.

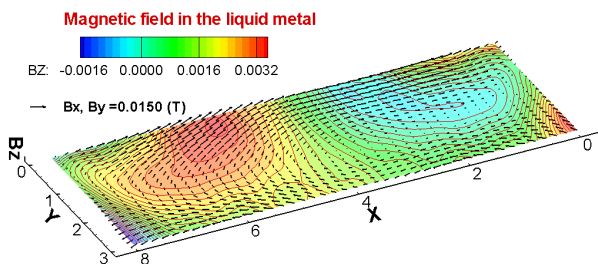


Figure 15. The computed magnetic field at the top of liquid metal for the 180 kA bus network.

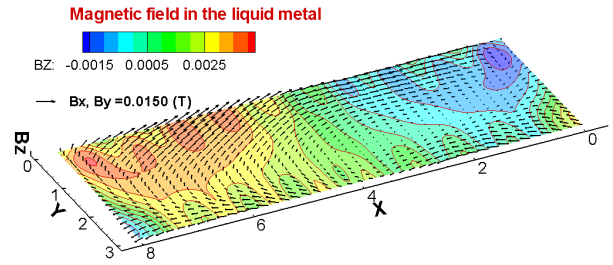


Figure 16. The computed magnetic field at the bottom of liquid metal for the 180 kA bus network.

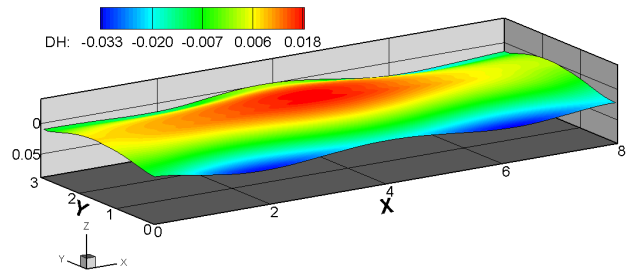


Figure 17. Initial surface of the liquid metal, 5s, when channels are accounted.

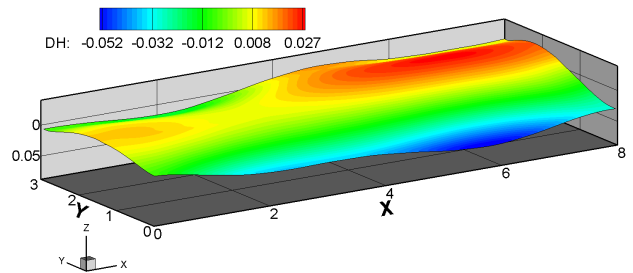
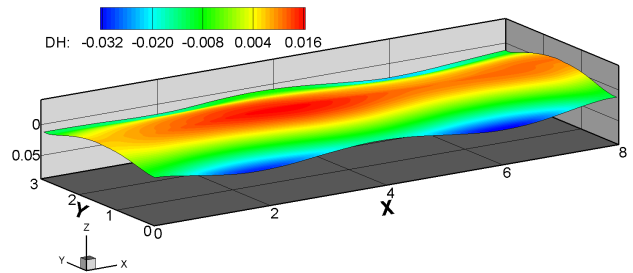


Figure 18. Sloshing wave development with the channel effect.

However, the distribution of the magnetic field in this cell is more concentrated in the middle of the cell, which leads to an unstable wave development, as illustrated in the Figure 18. The time history and the Fourier power spectra are shown in the Figure 19. This Figure shows also the instructive comparison with the wave development in case without the presence of the free electrolyte channels.

Without the inclusion of the electrolyte channels with free surface the instability sets in more easily, and the time when the wave crest reaches the anode bottom is shorter. The instability type in the case without the channels is the classical rotating wave (see Figure 20),

as described in the theoretical papers [5-7]. The presence of the electrolyte channels changes the instability type, which resembles a ‘sloshing’ wave concentrated along the middle longitudinal line of the cell. The Fourier power spectra clearly demonstrate the difference in the wave frequencies: a single peak for the case with the channels, and at least two dominant wave frequencies for the case not accounting for the channels.

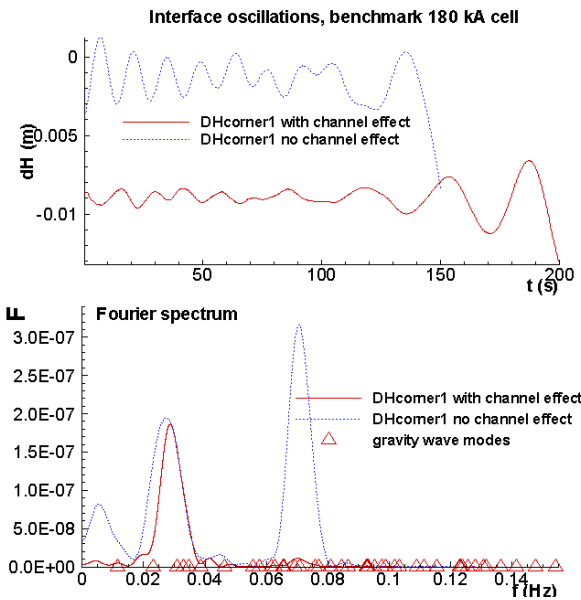


Figure 19. The channel effect on the unstable interface development and the respective Fourier power spectra.

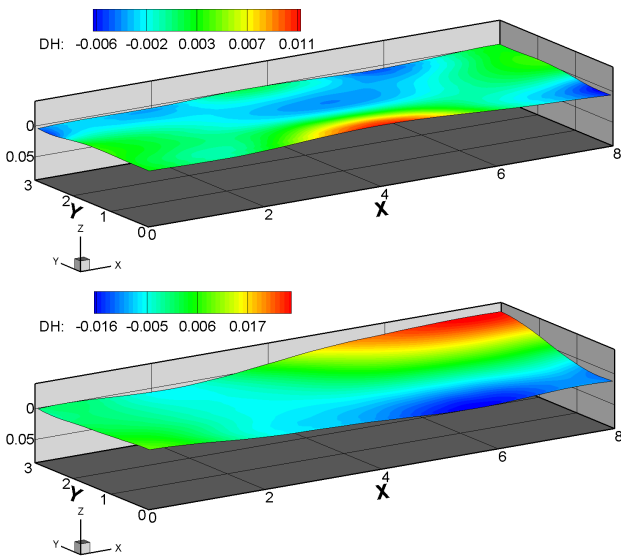


Figure 20. Rotating wave development without the channel effect.

Conclusions

MHD model software for the cell stability analysis was updated to take into account the deformed bottom and top surfaces with the free channels filled with liquid electrolyte.

Good comparisons to the previously published ‘benchmark’ tests were presented for the stationary case.

For the 180 kA cell, the non-linear cell stability results show that the presence of the free channels affects the cell stability, making it relatively more stable. The well known rotating wave instability is observed without the channel effect. With the channels the instability of the surface wave is of different type, resembling a sloshing wave.

References

1. D.S. Severo, V. Gusberti, A.F. Schneider, E.C. Pinto and V. Potocnik, “Comparison of Various Methods for Modeling the Metal-Bath Interface”. In *Proceedings of TMS Light Metals* (2008), 413-418.
2. R. Moreau and J.W. Ewans. An analysis of the hydrodynamics of aluminium reduction cells. *Journal of Electrochemical Society*, 131 (1984), no. 10, 2251-2259.
3. C. C. Mei. *The Applied Dynamics of Ocean Surface Waves* (World Scientific, 1989).
4. A.K. Rastogi and W. Rodi. Prediction of heat and mass transfer in open channels. *J. Hydraulics Division ASCE*, HY3 (1978), 397-420.
5. Urata, N., Mori, K. and Ikeuchi, H. Behavior of bath and molten metal in aluminium electrolytic cell. *Keikinzo*, 26 (1976), no. 11, 573-600.
6. A. D. Sneyd and A. Wang. Interfacial instability due to MHD mode coupling in aluminium reduction cells. *J. Fluid Mech.*, 263 (1994), 343-359.
7. V. Bojarevics and M. V. Romerio. Long waves instability of liquid metal-electrolyte interface in aluminium electrolysis cells: a generalization of Sele’s criterion. *Eur. J. Mech., B/Fluids*, 13 (1994), no 1, 33-56.
8. H. Sun, O. Zikanov, B. A. Finlayson and D. P. Ziegler. The influence of the basic flow and interface deformation on stability of Hall-Herault cells. *Light Metals 2005*, (TMS, 2005), 437-441.
9. V. Bojarevics and K. Pericleous, “Shallow Water Model for Aluminium Electrolysis Cells with Variable Top and Bottom”. In *Proc. TMS Light Metals* (2008), 403-408.
10. V. Bojarevics and K. Pericleous, “Comparison of MHD Models for Aluminium Reduction Cells”. In *Proceedings of TMS Light Metals* (2006), 347-352.